Land and Water Science
61c Leet Street
Invercargill 9810
New Zealand

03 214 3003
www.landwaterscience.co.nz

27th June 2019

Mapping of Northland's hydric soils, wetlands, and water bodies

Envirolink Grants: 1955-NLRC214 + 1956 NLRC215

Prepared for Northland Regional Council

June 2019

Prepared by: Dr Clint Rissmann, Jessie Lindsay, Matt Couldrey, and Dr Lisa Pearson

Internal reviewer: Dr Monique Beyer

External reviewer: Dr Richard Muirhead, AgResearch

1 Introduction

Approximately 95% of Northland's original wetlands have been lost. Northland Regional Council (NRC) have been trying to improve knowledge of existing wetlands, to better understand how best to prevent further loss, to identify suitable restoration sites, and to provide landowners with better advice for wetland protection and management. There has also been a transition towards finer scale mapping of the region's natural resources, including understanding the landscape controls over sediment loss, movement, and capture (Rissmann et al., 2018). The correlation between wetland loss and problematic sedimentation levels (Northland's main water quality issue) is not fully understood. However, combining sediment tracking and mapped current and potential wetlands (hydric soils) has potential to contribute significantly towards reducing sedimentation levels. This study aims to maximise the use of existing information and outputs to benefit multiple regional council teams (e.g. Land management, Planning and Policy, Biodiversity, Consents, State of Environment and the Hydrology team).

Radiometric data combined with remotely sensed data sets (Sentinel imagery) provides an integrated and more resolved layer of wetland extent and type than currently exists. Specifically, radiometrics provide an ability to look beneath the current vegetative cover whereas sentinel imagery data sets based on reflectance support above ground classification of ground cover and vegetative type. Currently there is no equivalent information or classification product available to NRC able to provide both below and above ground classification.

This letter report summarises the methodology and validation of radiometric and satellite imagery for the purposes of wetland mapping. The integration of these two datasets will occur at a later stage in the work plan.

1.1 Workplan

This work is separated into two phases. Phase 1 (1955-NLRC214) sought to develop a method to map at relatively high resolution the extent and type of wetlands across the Northland Region utilising existing airborne radiometric and sentinel imagery. Phase 2 (1956 NLRC215) proposed to test the methodology against existing inventories of wetlands and organic soils. Here the theory, method, validation and outputs are combined into a short report. Development of an interactive geospatial package that integrates both the radiometric and sentinel imagery is the subject of future work (Phase 3) via a contract between NRC and Land and Water Science.

1.2 Workshops with NRC

The primary output of these Envirolink MAGs were workshops with NRC staff. Two formal and four informal workshops were held with Northland Regional Council staff to outline the concept, development and performance of the preliminary wetland and hydric soil classification. Workshops enabled the developers to seek technical feedback and as a basis for ground truthing interpretations with expert field staff with a strong working knowledge of the region. Staff involved in the workshops included a mix of policy, science and extension staff and managers.

2 Radiometric Based 'Wet-land' Classification

Airborne gamma ray spectroscopy is a geochemical method used for understanding natural gradients in geological provenance, weathering, landscape stability and wetness (Løvborg, 1984; Pickup and Marks, 2000; Wilford, 2012; IAEA, 2003; Beamish, 2013b, 2014). Gamma rays are high energy photons (particles of light) with energies ranging from 10^4 ev (electron volts) to 10^7 ev. As applied to airborne radiometric survey, gamma ray detectors, i.e., scintillators, count the number of photons of a given spectral energy range to measure radioactivity from naturally occurring radioactive materials within the uppermost portion of the earth's surface (c. 300 – 1,000 mm). In the airborne survey of Northland, the detector is flown at a height of 60 m above ground level and along a 200 m line spacing with a tie line of 2000 m to produce a ground-based resolution of 50 x 50 m or 0.25 Ha (Stagpoole et al., 2012).

For airborne gamma ray spectroscopy (AGRS), the survey method employs a gamma ray detector (NaI scintillator) tuned to detect ^{40}K and estimate uranium (^{238}U) and thorium (^{232}Th) through the radon daughter ^{214}B in its decay chain and thorium (^{232}Th) via ^{208}Tl in its decay chain. Potassium (^{40}K) is measured directly at 1.461 MeV (megaelectronvolt). Secular equilibrium in the decay chains of ^{238}U and ^{232}Th is assumed and the ground concentration results are reported as equivalent uranium (eU, ppm) and equivalent thorium (eTh, ppm). Potassium is reported as %K.

Geological provenance (rock and sediment type), weathering intensity and landscape stability gradients are inferred from spatial gradients in K, eU, eTh concentration, mass ratios (e.g. Th/K) and Total Count (counts per second (cps) logged by the detector). However, effective radiometric interpretation necessitates an appreciation of the geological setting, morphometric and hydrological controls over the observed gradients in gamma ray spectra and total count (Pickup and Marks, 2000; IAEA, 2003; Rawlins et al., 2007, 2009; Gatis et al., 2019). Effective application of AGRS therefore requires an integrated knowledge of petrochemistry, geochemical weathering, structural geology and associated geomorphic gradients.

2.1 Gamma Ray Attenuation for Peat and Hydric Soil Mapping

The mapping of peat and hydric soil extent using airborne gamma ray spectroscopy relies on an assessment of the attenuation of gamma radiation by the three-phase system, air-liquid(water)-solid, that constitutes rock and soil (Løvborg, 1984; Beamish, 2013a,b, 2014; 2016; Gatis et al., 2019; Rawlins et al., 2007, 2009). This differs from geological, soil and landscape stability mapping which is focussed on interpreting the spatial variation in K, eTh, eU and relevant mass ratios (i.e., eU/eTh, K/eTh) with regards to geological and geomorphic gradients.

Gamma ray attenuation primarily occurs via incoherent scattering of gamma rays by electrons associated with earth materials and water. The degree of attenuation is determined by the density of electrons which is a product of both the dry bulk density and the volumetric water content of the earth material[1]. Importantly, relative to rock and soil, water has a greater electron density and as such is a stronger attenuator of gamma rays[2] (Løvborg, 1984).

Therefore, the maximum gamma ray signal (S) emitted from a particular depth in centimetres (d) is given by:

$$S(d) = (1 - \exp(-0.046*\rho*d))*100 \qquad \text{(Eq. 1)}$$

where ρ is the dry bulk density of the material in $g.cm^{-3}$ (Taylor et al., 2002). The factor 0.046 is an assumed mass attenuation coefficient for the material and the energy considered. This expression indicates that about 90% of the radiometric signal comes from the top 30 cm of the soil when the average dry bulk density is 1.6 $g.cm^{-3}$ (Figure 1). For a lower dry bulk density and for the very low densities of some organic soils (c. 0.1 g. cm^{-3}) the emission profile will be deeper c. ≥100 cm. These theoretical emission depths represent maximum values and are modified by the volumetric water content. Laboratory and field-based studies note a quasi linear relationship between volumetric water content and gamma ray attenuation, with a 10% increase in attenuation for every 10% increase in volumetric water content (Grasty and Minty, 1995; Cook et al., 1996; IAEA, 2003).

Figures 1a and 1b from Beamish (2013a) provide examples of the relationship between soil dry bulk density and volumetric water content. Specifically, reference mineral soils of lower bulk density (1.1 $g.cm^3$) have a shallower attenuation curve than mineral soils with a higher bulk density (1.6 $g.cm^{-3}$). Also evident is that gamma ray attenuation approaches 100% for standing water with a depth of ≥0.9 m^3. Figure 1b displays attenuation curves for 5 soils and two different rock types in terms of

[1] A. As air is part of the airborne measurement it is ignored with the electron density governed by the dry bulk density and volumetric water content of the earth material; B. there is little variation in electron density for earth materials with different geochemical composition with the exception of ore grade deposits of heavy atoms with an atomic number > 30 (Løvborg, 1984).

[2] Waters greater electron density is due to the absence of a neutron within the nucleus of the hydrogen atom.

[3] Lakes >1 m deep are often used to assess the 100% attenuation base line in AGRS survey.

their degree of saturation with respects to water. As expected, there is a strong correlation between porosity, density and volumetric water content and resultant gamma ray attenuation. At full saturation, attenuation approaches 100% for the peat soil. Most critical here is that water content is the dominant factor governing attenuation in low density soils such as peat.

Another relevant feature of low-density organic soils is the lesser concentration of radiogenic minerals. This equates to a lower emanation power relative to mineral soils. Due to the strong attenuation capacity of water and the naturally low radionuclide concentration or organic matter, areas of organic and especially wet organic soils are commonly associated with the lowest gamma ray emanation signature or Total Count. In short, the attenuation of gamma ray emission by organic soils are highly detectable (Beamish, 2013a,b, 2014, 2016; Gatis et al., 2019).

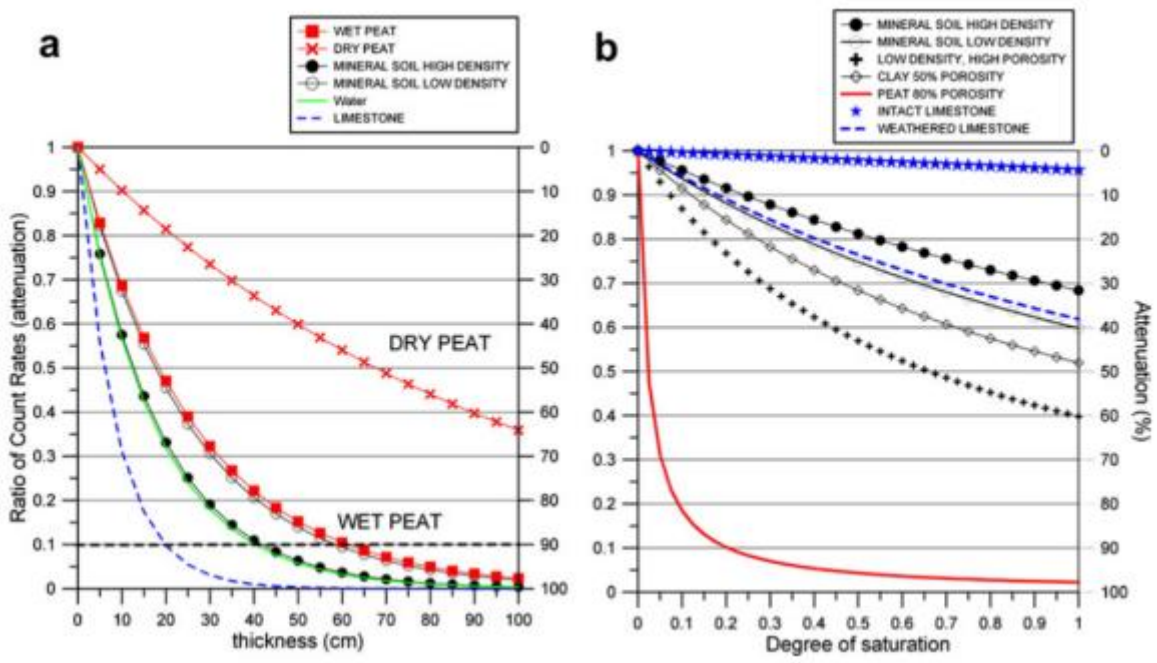

Figure 1: Theoretical attenuation behaviour of soil/bedrock types from Beamish (2013a). (a) Variation with thickness assuming a uniform half-space. A 90% attenuation level is shown by the horizontal dash line. (b) Variation with degree of saturation (soil moisture or moisture content).

2.2 Attenuation Relative to Geology

The relative radiogenic content of rock or soil and its emanation strength varies according to the provenance of the inorganic minerals, their degree of weathering and any attenuation associated with material density and water content (Rawlins et al., 2007; 2009; Beamish, 2013a,b, 2014, 2016; Gatis et al., 2019). As such, although, areas of peat consistently show low radiometric counts due to strong attenuation, equivalent gradients in the magnitude of attenuation are seldom constant across soil and rock materials of varying provenance and weathering intensity (Beamish, 2015; Gatis et al., 2019). Specifically, a peat wetland formed in and over top of a high (e.g. rhyolite or felsic greywacke) Total Count parent material will exhibit a steeper equivalent relative attenuation rate than a peat wetland formed in and over top of a low Total Count (e.g. basalt) bedrock. As such, it is optimal to provide an assessment of attenuation that is relative to the provenance and degree of weathering of

earth materials when attempting to provide a regional scale classification of perennially wet land (Rawlins et al., 2007, 2009; Beamish, 2013a,b, 2014, 2016; Gatis et al., 2019).

2.3 Materials and Methods

Airborne gamma ray survey data for the Northland region was downloaded from New Zealand Petroleum and Minerals' online data base. A discussion of the survey technique and processing is provided in "Northland airborne magnetic and radiometric survey: a geological interpretation" a GNS Science Report 2011/54 (Stagpoole et al., 2012). Downloads included Total Count (counts per second), potassium (%K), equivalent Thorium (Th), equivalent uranium (U) and the Th/K and U/Th mass ratios. Airborne gamma ray survey data for the Northland region is shown as a ternary diagram in Figure 2.

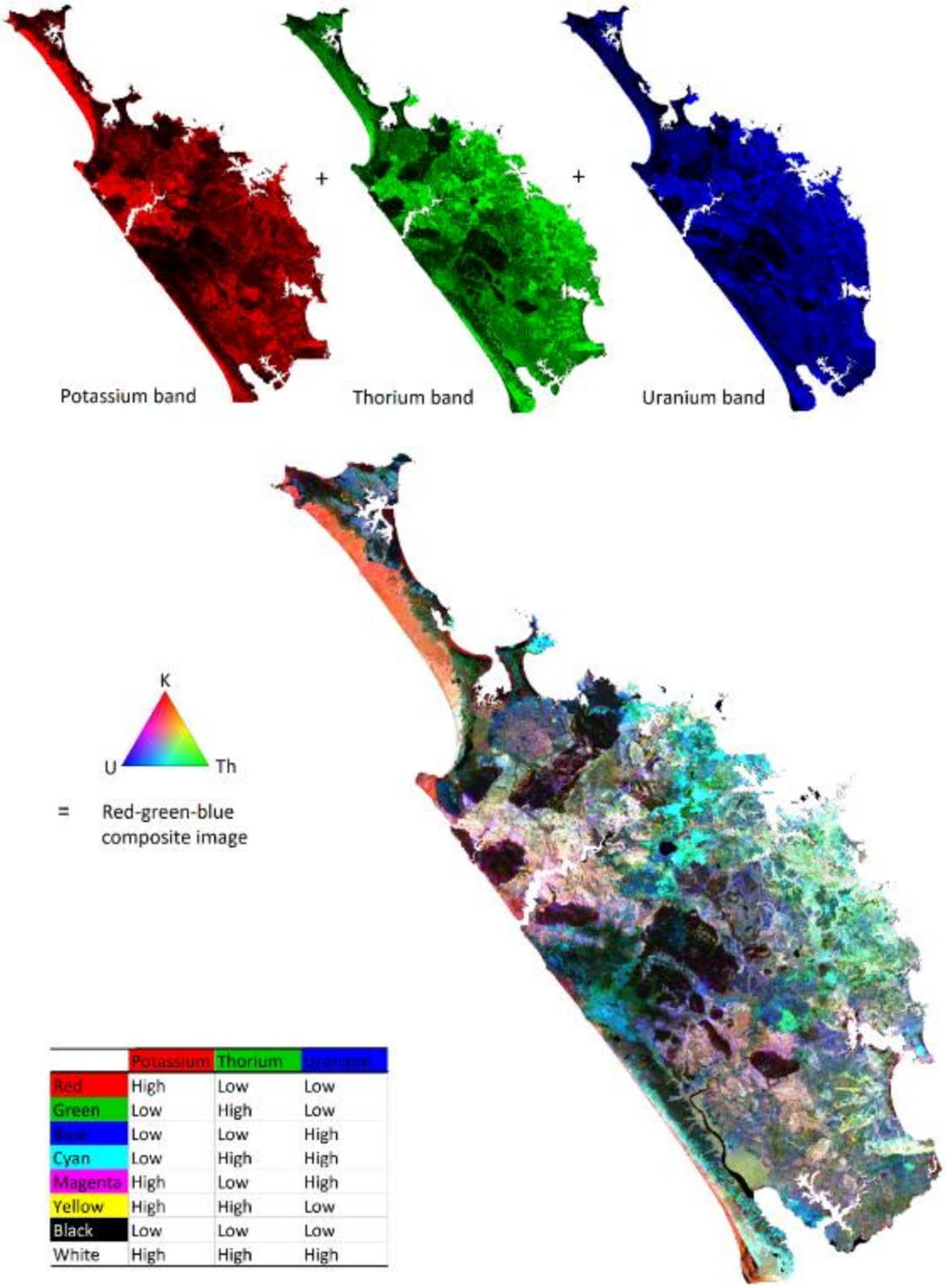

	Potassium	Thorium	Uranium
Red	High	Low	Low
Green	Low	High	Low
Blue	Low	Low	High
Cyan	Low	High	High
Magenta	High	Low	High
Yellow	High	High	Low
Black	Low	Low	Low
White	High	High	High

Figure 2: Airborne Gamma-Ray Spectroscopy (AGRS) ternary for the Northland Region (NZP&M, 2011). Table of colours produced by variable mixing of K, eTh and eU.

Total Count is the preferred resource for identifying and mapping peat wetlands due to the higher signal to noise ratio (Beamish, 2014; Figure 3). A small number of negative values and all 0 counts were set to a count per second (cps) of 1 to enable estimation of percent attenuation and for the purposes of log transformation and z-scoring of the raster layer for potential image analysis (see

Gatis et al., 2019). Table 1 summarises the Total Count zonal statistics for the Northland region. Please note that 0 cps is consistent with 100% attenuation or saturation by water (see above).

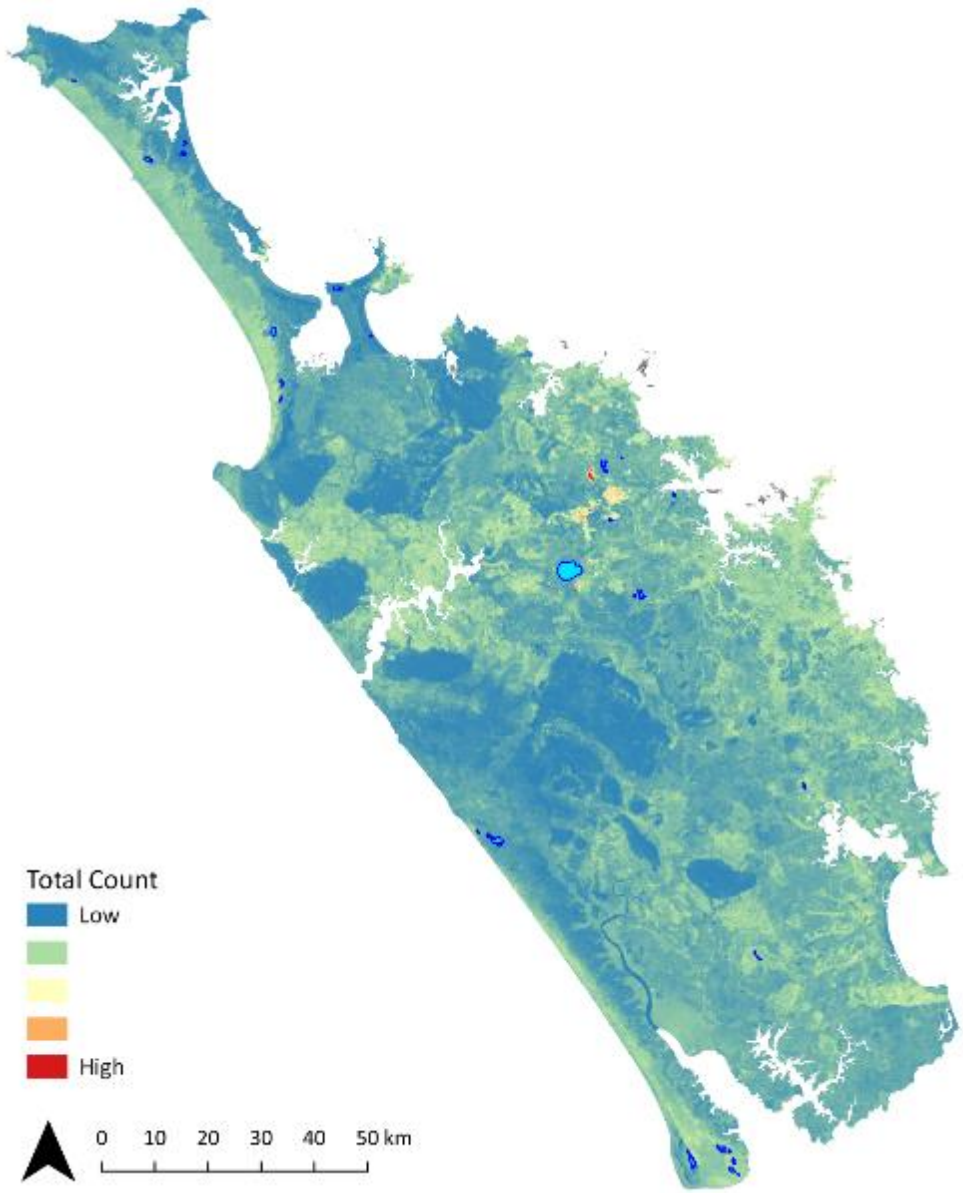

Figure 3: ARGS Total Count (counts per second) for the Northland Region.

Table 1: Summary statistics of total count for the Northland Region (cps).

	Mean	Median	Standard dev.	Minimum	Maximum
Northland	600.6	581.7	322.6	1	5870.9

To provide an assessment of attenuation that is relative to the provenance and degree of weathering of earth materials for a regional scale classification of perennially wet land, the primary bedrock signatures need to be identified. The primary geochemical signature of the main rock types across Northland were determined by isolating the steepest and most rugged classes within the radiometric and terrain-based data driven geological classification of Rissmann et al. (2018; Figure

4). The data-driven classification of Rissmann et al. (2018) was also used to generate geological boundaries for those units that are not well defined at the resolution (1:250,000) of existing geological maps (QMAP; Isaac, 1996; Edbrooke, 2001; Edbrooke and Brook, 2009; Figures 5 - 7). The steepest and most rugged terrain classes within the geological classification of Rissmann et al. (2018) that were geochemically the most indicative of relatively unweathered rock or sediment material were isolated and their zonal statistics calculated (Table 2). For example, classes within the pre-defined Tangihua Basalts associated with the steepest slopes and most rugged terrain were used to derive mean, median, maximum and minimum Total Count values. Zonal statistics were also determined for polygons associated with pre-existing wetland and lake polygons [4]. For depositional sediments those with the highest elevation were isolated in order to limit the influence of shallow floodplain water tables over the attenuation[5].

[4] Where primary bedrock is the least weathered rock or sediment material. Such material is readily identifiable from AGRS spectra and is further resolved by the inclusion of topographic factors such as slope and terrain ruggedness.

[5] A strong positive spatial correlation between alluvial terrace elevation and Total Count was observed. This relates to the impact of higher water tables at lower elevations over attenuation.

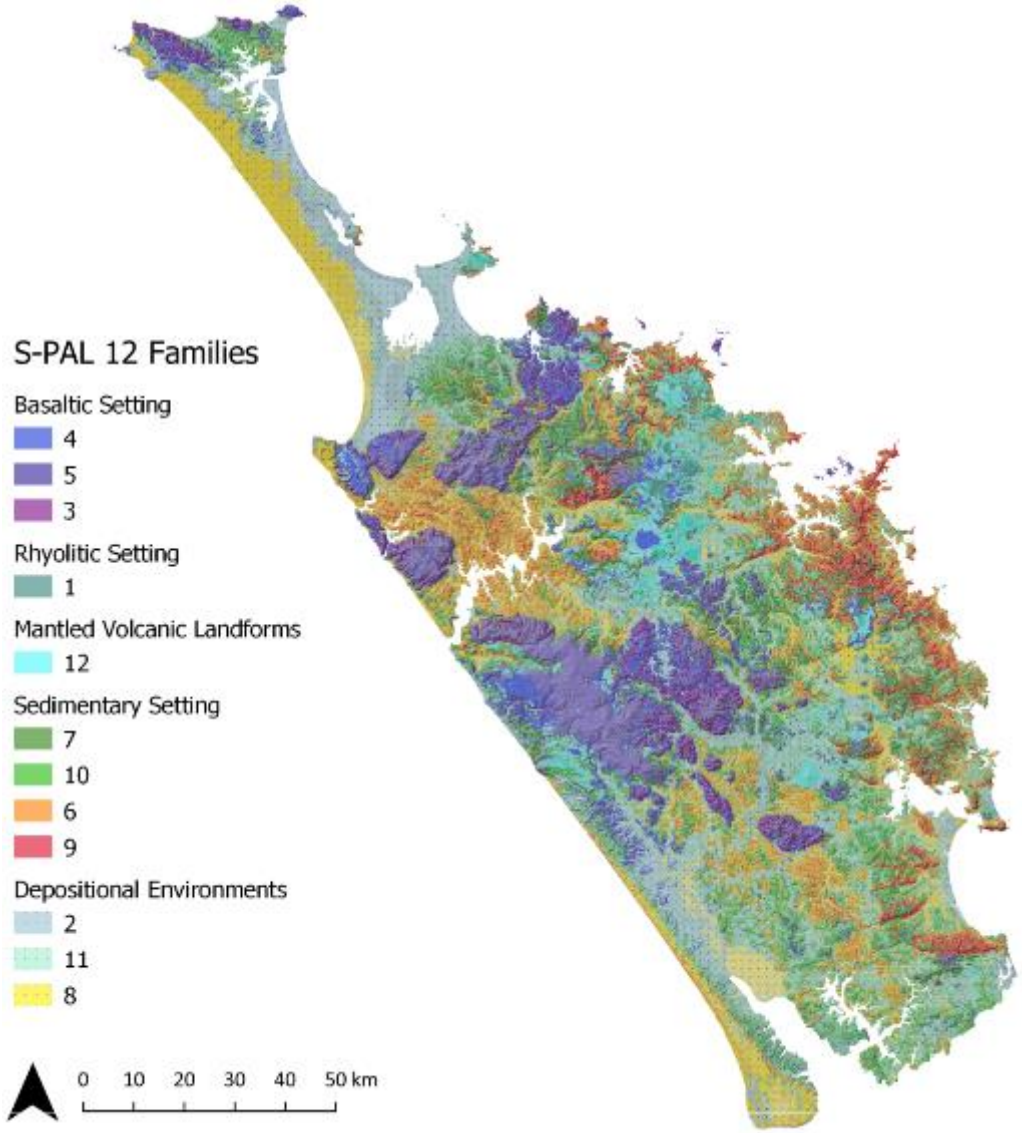

Figure 4: Data driven geological (S-PAL$_{35}$ genetic classification) classification of the Northland region into 12 main geological families and 35 individual classes (Rissmann et al., 2018). This data driven classification shows a strong correspondence to existing geological maps but with the benefit of greater resolution (50 x 50 m) and finer grained resolution of within geological unit variation.

Table 2: Total count values for all primary bedrock and sediment signature classes, wetlands and lakes (cps).

Primary Bedrock Classification	Total Count mean	Total Count median	Total Count standard dev	Total Count min	Total Count max
Basaltic Facies					
Tangihua Complex	125.4	108.3	70.2	1	798.0
Waipoua Basalt	260.0	244.4	109.4	25.7	937.0
Basaltic (Family 3,4,5)	318.6	325.0	88.1	1	950.6
Sedimentary Facies					
Punakitere Sandstone	1,302.8	1,341.7	212.7	506.3	1,860.0
Waipapa Group + Caples Group	1,268.4	1,253.3	268.3	364.7	3,121.9
Awhitu Group	236.9	233.9	69.8	1	487.6
Family 12	705.8	665.5	235.4	74.3	1,833.2
Sedimentary high TC (Family 6 and 9)	864.2	808.8	206.5	101.0	3,241.6
Sedimentary low TC (Family 7 and 10)	543.6	541.7	101.5	39.4	1,131.6
Rhyolite Facies					
Rhyolite (1a)	1,896.9	1,709.7	576.8	430.3	5,870.9
Rhyolite (1b)	2,450.7	2,393.2	728.1	1,299.9	5,288.7
Depositional Environments					
Family 2, 8, 11	626.6	604.3	244.8	1	1,660.7
Wetlands (Top150)	317.4	280.4	232.5	1	2,815.2
Lakes (Topo 1:50,000)	172.1	80.1	215.3	1	1,237.5

Median values of the primary bedrock and sediment Total Count were considered most representative and were used to derive a percentage deviation (attenuation) from the primary bedrock signature[6]. Attenuation for each pixel was calculated by dividing each individual pixel within the 12 geological families by their respective primary bedrock/sediment median and then multiplying by 100.

[6] Median values are less influenced by anomalous Total Count values that occur in association with fault zones and pockets of mineralisation.

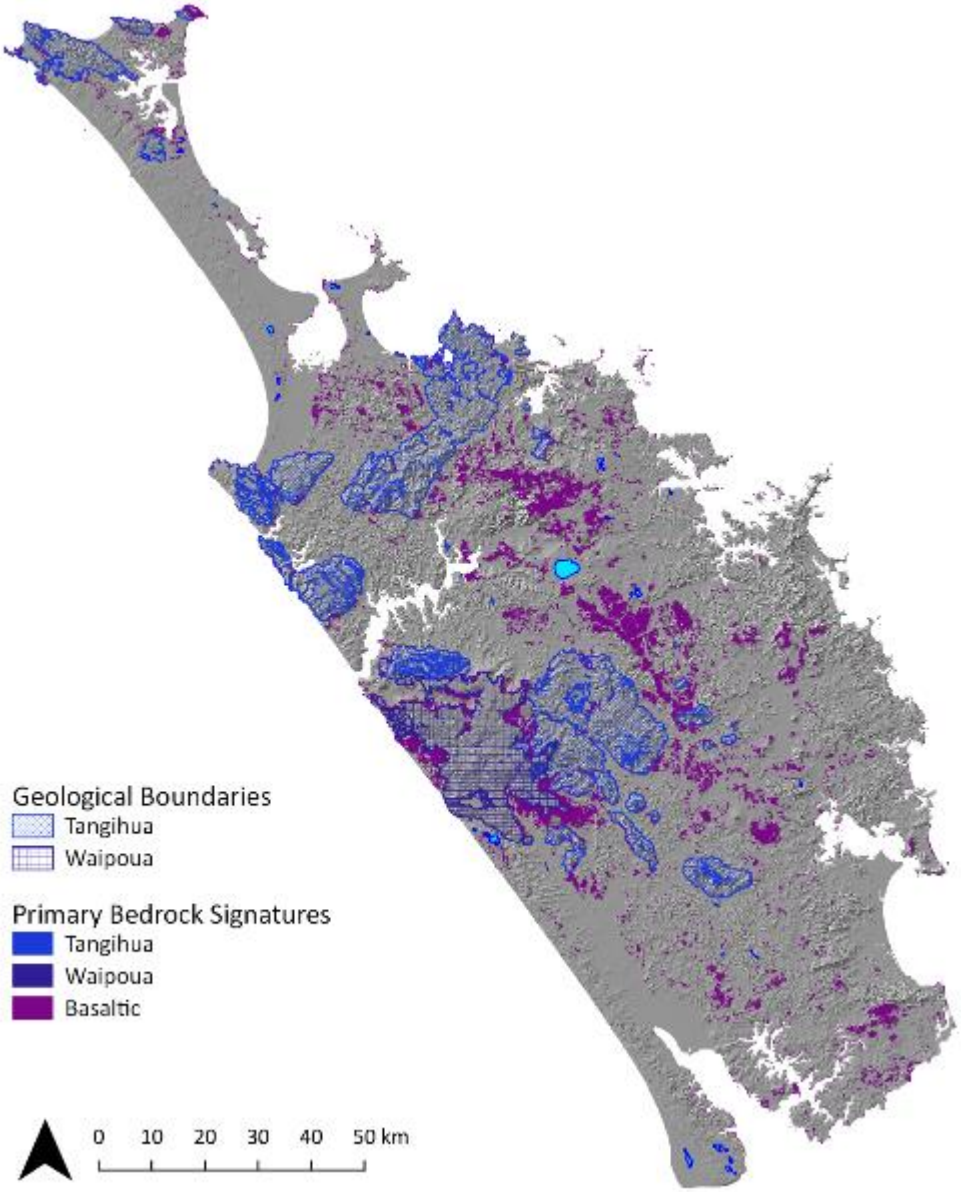

Figure 5: Geological boundaries from Q-Map and associated primary bedrock geochemical classes for Tangihua Complex and Waipoua Basalts. Primary bedrock geochemical classes for non-Tangihua and Waipoua volcanics also shown. Within each unit the classes associated with a primary bedrock geochemical signature were isolated using the data-driven geological classification of Rissmann et al. (2018) and their zonal statistics calculated.

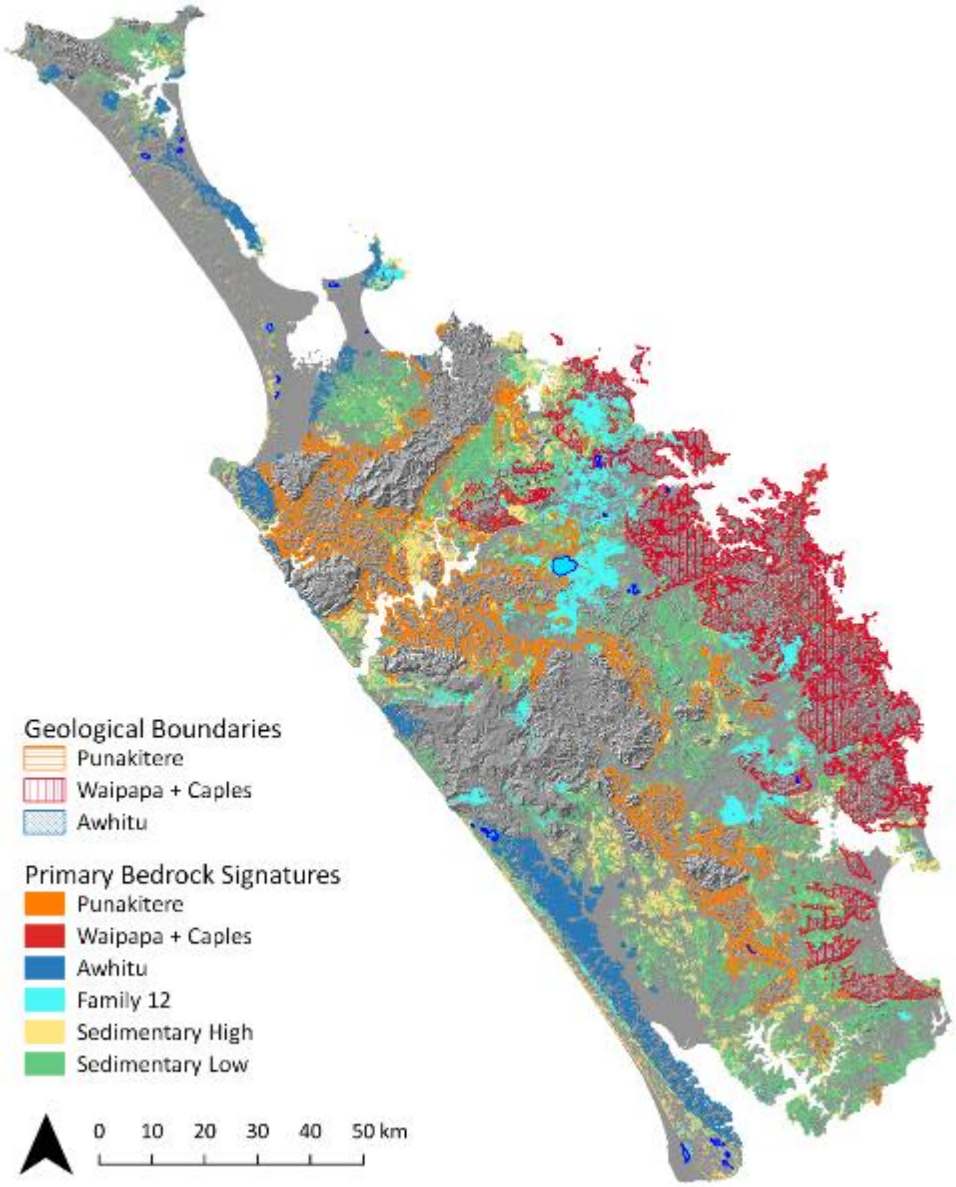

Figure 6: Geological boundaries from Q-Map and associated primary bedrock geochemical classes (after Rissmann et al., 2018) for sedimentary rocks. Within each unit the classes associated with a primary bedrock geochemical signature were isolated using the data-driven geological classification of Rissmann et al. (2018) and their zonal statistics calculated.

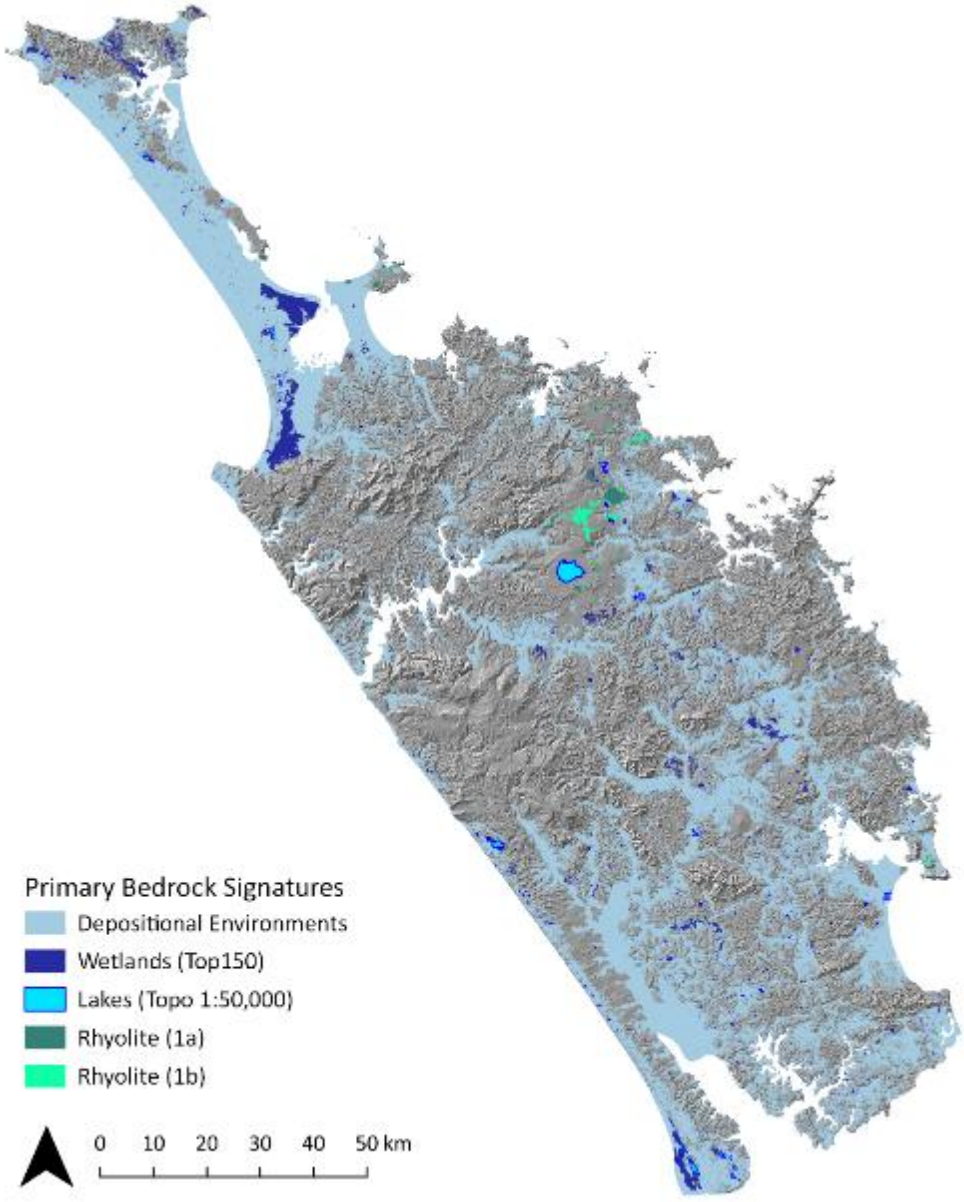

Figure 7: Extent of depositional classes (aeolian and alluvial), lakes, wetlands and rhyolite extrusives after Rissmann et al. (2018). For the depositional and rhyolite families those classes associated with a primary bedrock geochemical signature were isolated and their zonal statistics calculated.

A map of % attenuation relative to the provenance and degree of weathering of earth materials for the Northland region is provided in Figure 8. The mean and median attenuation % within all geological families are listed in Table 3. Zonal statistics for % attenuation are also provided for pre-existing wetland and lake polygons.

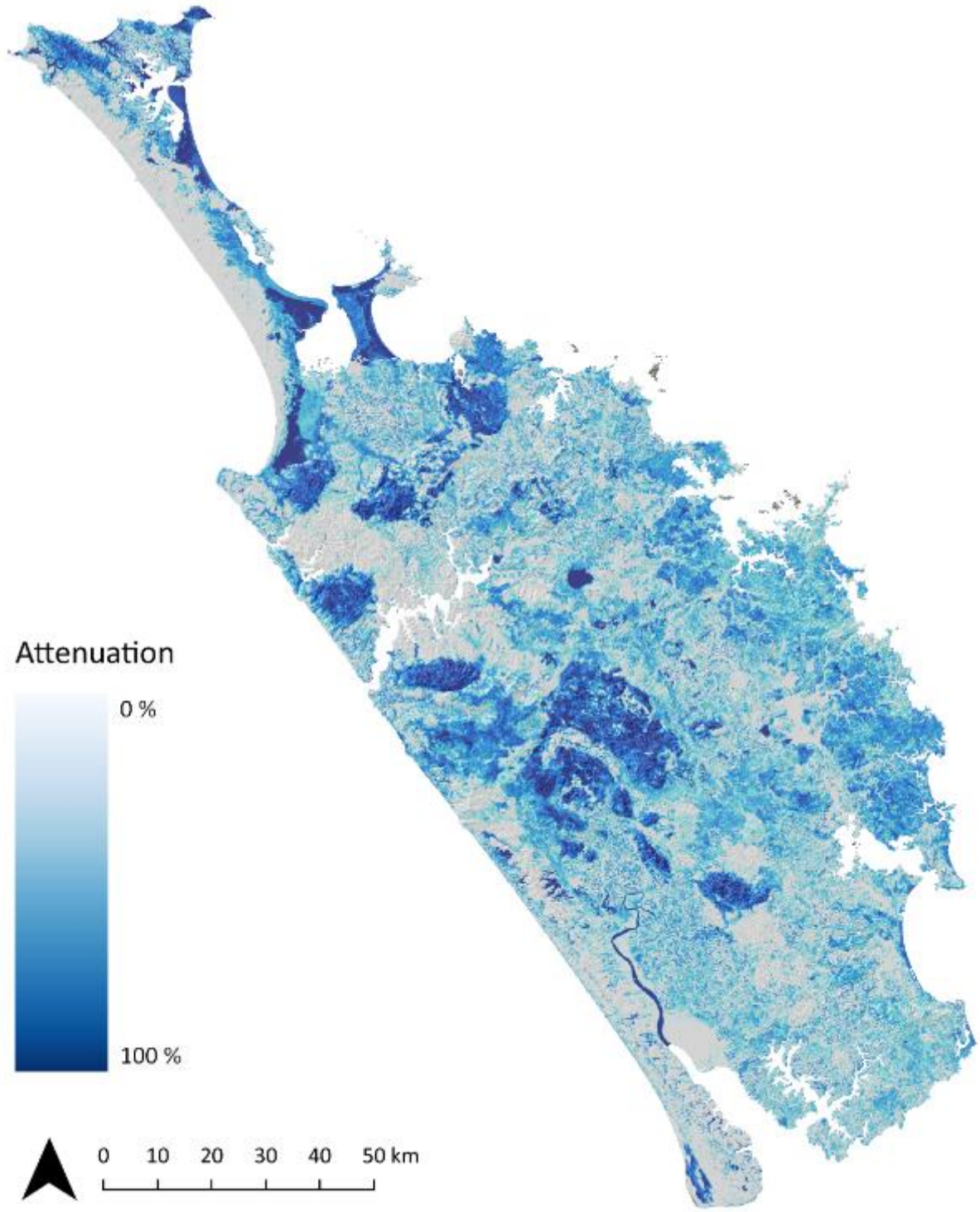

Figure 8: Relative attenuation (%) layer for Northland. Where 100% saturation is associated with saturation of porous media by water.

Table 3: Attenuation % values by geological families and for wetlands and lakes.

	Attenuation % mean	Attenuation % median
Basaltic Facies		
Tangihua Complex	74.7	81.5
Waipoua Basalt	69.7	73.1
Basaltic (Family 3,4,5)	68.9	68.2
Sedimentary Facies		
Punakitere Sandstone	55.1	55.2
Waipapa Group + Caples Group	71.3	72.3
Awhitu Group	29.4	37.9
Family 12	60.5	62.3
Sedimentary high TC (Family 6 and 9)	65.1	71.3
Sedimentary low TC (Family 7 and 10)	56.5	55.3
Rhyolite Facies		
Rhyolite (1a)	51.1	53.6
Rhyolite (1b)	62.0	68.8
Depositional Environments		
Family 2, 8, 11	62.1	63.2
Wetlands (Top150)	87.0	89.8
Lakes (Topo 1:50,000)	87.0	93.7

The % attenuation layer is still influenced by geology at a regional scale, however when viewing within a geological family and/or at property scales these limitations are minor. Further refinement of the primary bedrock signatures could be undertaken for low total count rock units such as the Tangihua Basalts and Awhitu Group (Neogene sedimentary). Here due to naturally low radioactivity and dense vegetation cover, radiometric signals may be partially masked by vegetative cover. This is less of an issue for other rock units which have naturally higher total count.

3 Satellite Based Wetland Vegetation Classification

Remote sensing has previously been used to map and monitor wetlands. Satellite data can provide data over a long-time frame at frequent intervals, providing an economical and time efficient method for monitoring wetlands compared with field mapping over large areas. Previously satellites, such as the Landsat series, have been used to map wetlands but due the low spatial resolution some homogeneous wetland areas, specifically along the coastlines are unable to be easily identified. The pixels in these areas were found to contain multiple land cover types of different proportion (Civco et al., 2006). Sentinel imagery can help improve the mapping of these areas with the use of 10 m spatial resolution and increased spectral resolution in the Near Infra-Red (NIR). The small pixel cell and increased spectral resolution allows for finer details of different vegetation types to be extracted from these areas.

Figure 9 demonstrates a workflow method to identify the boundaries of wetlands using object-based imagery analysis (OBIA) and the spectral signature within the segmented boundaries to classify the vegetation type of the wetland. For the purpose of this study we have used the 2016 LUCAS wetland polygons which are derived from a combination of Landsat and Sentinel imagery.

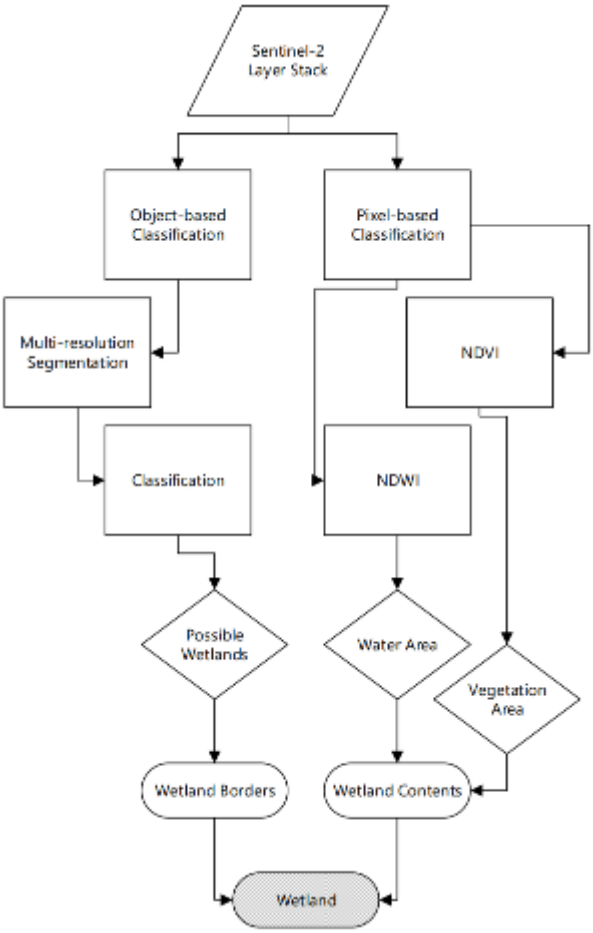

Figure 9: Wetland classification workflow as outlined in Kaplan and Avdan (2017).

3.1 Vegetation spectral signature for the identification of vegetation type

Vegetation has a unique spectral signature, but different types of vegetation differ in their reflectance. Plants that are stressed or diseased can also be identified by their distinct spectral signatures. The leaf pigments, cell structure and water content all impact the spectral reflectance of vegetation. For example, deciduous trees have a higher reflectance in the NIR compared to conifers therefore vegetation types can be distinguished from satellite imagery.

In the visible bands the reflectance is relatively low as most of the light is absorbed by the leaf pigments (Figure 10). Chlorophyll strongly absorbs energy in the blue and red wavelengths and reflects more green wavelengths. Therefore, healthy vegetation appears green. For healthy vegetation, the reflectance is much higher in the NIR region than in the visible region due to the cellular structure of the leaves. Therefore, healthy vegetation can be easily identified by the high NIR reflectance and generally low visible reflectance. The reflectance in the shortwave infrared (SWIR) wavelengths is related to the water content of the vegetation and its structure. Water has strong absorption bands around 1.45, 1.95 and 2.50 µm. Outside these absorption bands in the SWIR region, reflectance of leaves generally increases when water content in the leaf decreases.

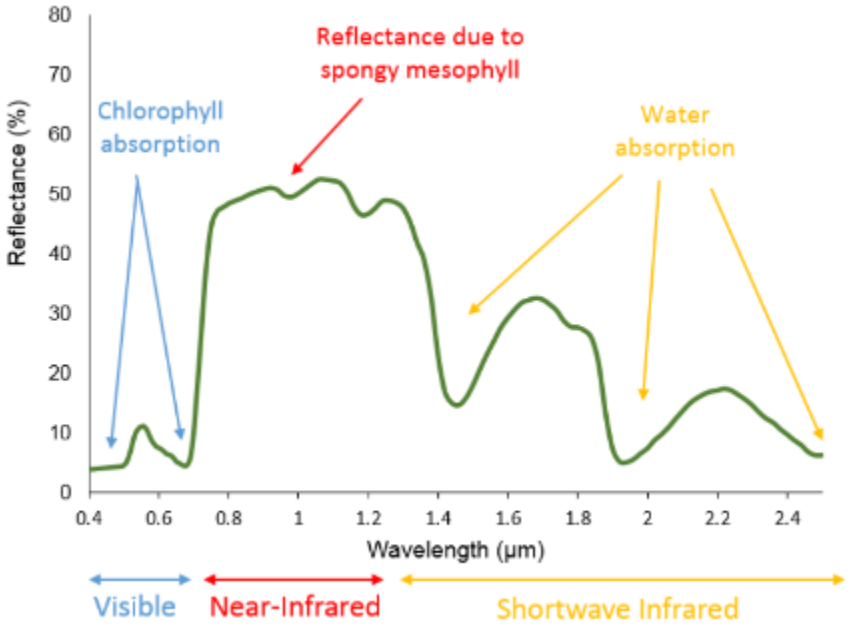

Figure 10: Vegetation spectral reflectance curve (From http://gsp.humboldt.edu/OLM/Courses/GSP_216_Online/lesson2-1/vegetation.html).

3.2 Sentinel imagery for vegetation identification

Sentinel imagery was selected over other optical satellites, such as Landsat 8 and ASTER, due to its ability to provide 10 m resolution in the visible and near infra-red band (VNIR). Landsat 8 is limited to 30 m resolution and ASTER 15 m resolution. The accuracy and level of detail obtained from the use of optical satellite imagery for monitoring changes in vegetation is limited by the spatial resolution of the sensor, cloud free images and errors embedded in the data from the altitude/orbit of the satellite when scanning (Scherler et al., 2008).

The two Sentinel satellites (A and B) occupy the same orbit above Earth at an altitude of 786 km. They are separated by 180° giving a return rate over New Zealand of 5 days, or a 10-day return rate for each satellite, providing high resolution multi-spectral images and a more frequent return rate than Landsat or ASTER giving a greater pool of images to select cloud free data from.

Resolution is defined according to the satellites ability to discern differences in light intensity. The greater the resolution, the higher the accuracy of the image. Sentinel satellite imagery was selected from 3 different dates to obtain complete coverage of the Northland region in the 10 m bands (bands 4, 3 and 2 in the visible spectrum and band 8 in the NIR; Figure 11).

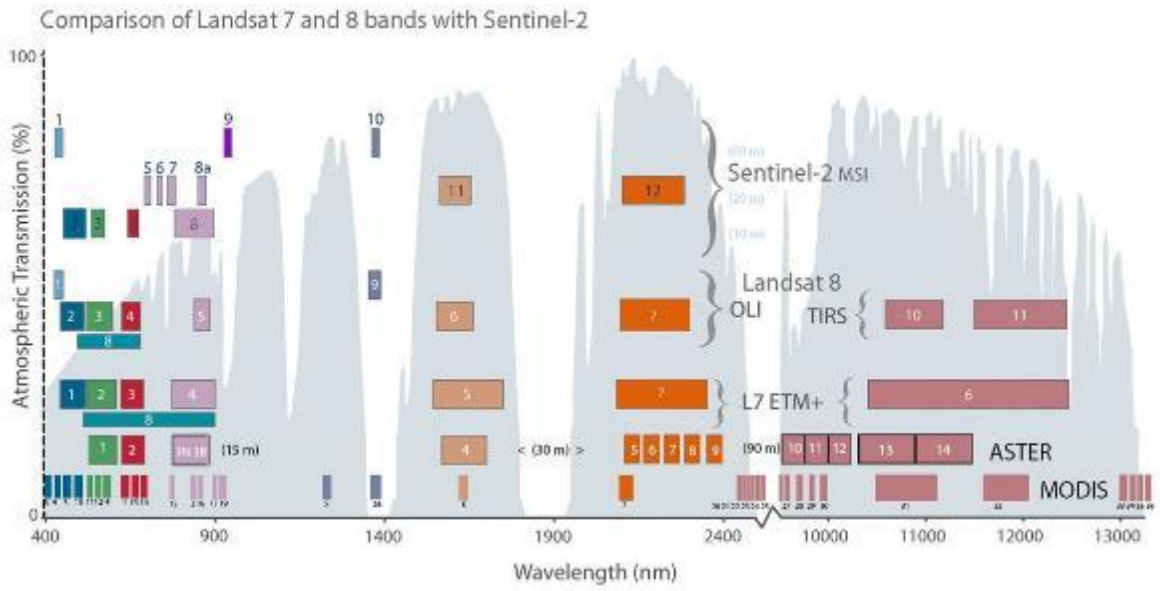

Figure 11: A comparison of the Sentinel-2 bands with Landsat, ASTER and MODIS showing. Figure retrieved from: https://twitter.com/USGSLandsat

3.3 Materials and Methods

To achieve a cloud-free image of the Northland region, imagery was mosaicked together from the 24th of April 2017, 29th of May and 21st of June 2018 (Figure 11). For full image details see Table 4.

Figure 12: Extent of satellite images identified in Table 5.

Table 4: Sentinel images mosaicked together to form the whole region.

Sentinel image	Image	Orbit	Cloud coverage assessment (%)
S2A_MSIL1C_20180621T223531_N0206_R072_T59HPB_20180622T013306	2	72	1.2
S2A_MSIL1C_20180621T223531_N0206_R072_T59HQA_20180622T013306	4	72	0.8
S2A_MSIL1C_20180621T223531_N0206_R072_T59HQB_20180622T013306	5	72	4.7
S2A_MSIL1C_20170424T222541_N0204_R029_T60HTF_20170424T222539	7	29	0.2
S2A_MSIL1C_20180529T222541_N0206_R029_T59HQV_20180529T234439	8	29	30.2

Northland Regional Council provided 185 polygons (11,835 Ha, <1% of the Northland region) containing 87 different vegetation combinations. These were simplified to 20 vegetation classes (Table 5).

Table 5: Vegetation types for the Northland Region.

Wetland type	Area (Ha)	Polygon count
Pine and ginger	4709.4	8
Bog	148.9	8
Sedge	83.2	14
Ginger	68.5	3
Natives and ginger	29.5	4
Rice grass	17.2	6
Californian bullrush	10.1	4
Kahikatea forest	8.5	1
Gumland	6.9	1
Grassland	6.4	8
Raupo	3.1	5
Reedland	2.3	8
Shrubland	2.1	6
Treeland	1.7	3
Rushland	0.8	6
Exotic	0.1	1

The points for the wetlands were loaded into SNAP 6.0.1, the European Space Agency's open sourced software for processing Sentinel imagery for analysis against the spectral signature. Spectral signatures were plotted for each of the vegetation classes classified by the Northland Regional Council. Figure 13 provides an example of the spectral signatures for the different wetland vegetation types. As many of the polygons contain mixed vegetation types the spectral differences between some vegetation types or with a vegetation class have a large range.

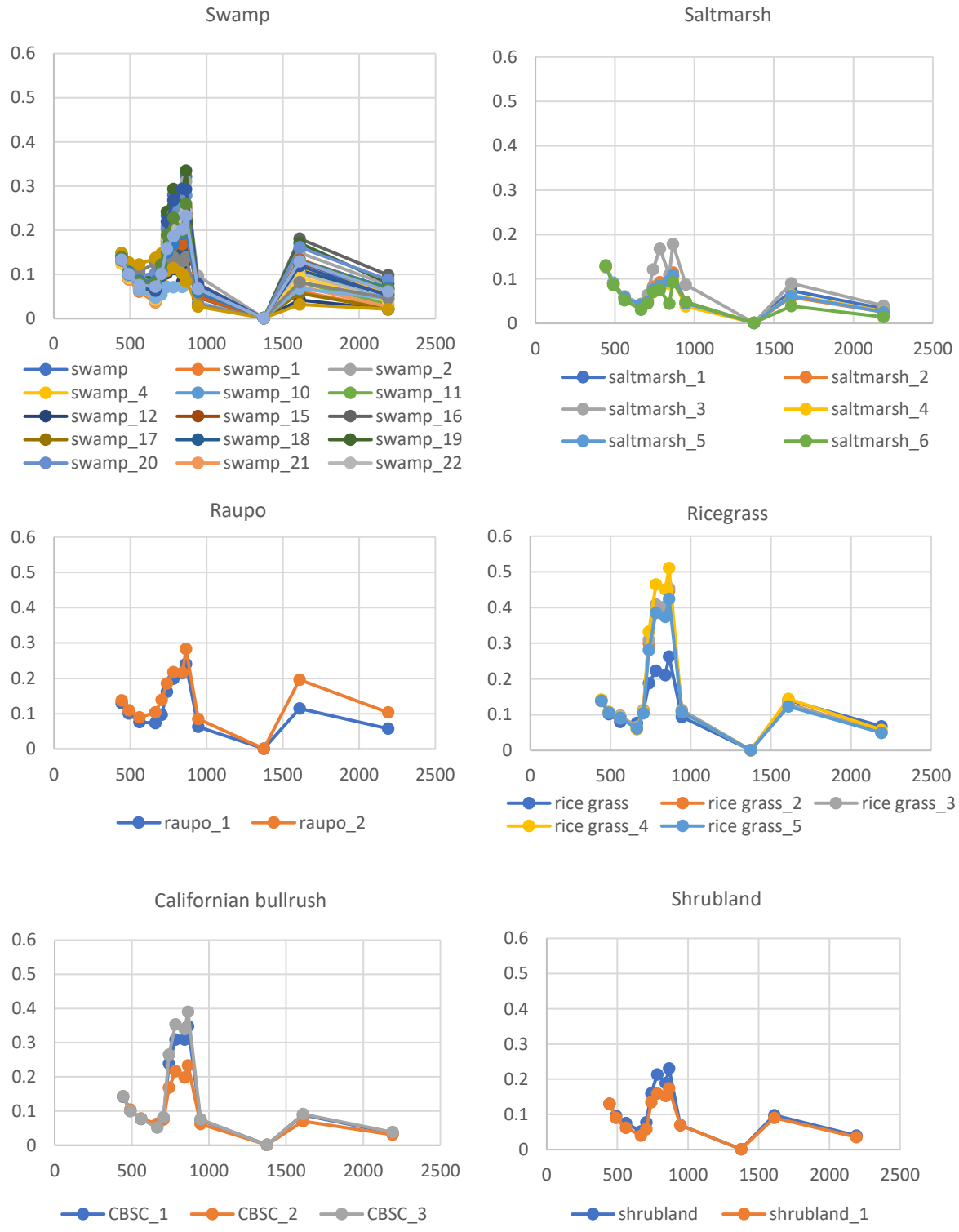

Figure 13: Spectral signature example from swamps, saltmashes, raupo and ricegrass vegetation types in Image 4 (of Figure 12).

The wetland polygons from the Ministry for the Environment Land Use and Carbon Analysis System (LUCAS) land use Layer (2016) was used as the outlines for the satellite-based wetland vegetation classification. The LUCAS land use layer was used to minimise the area of Northland requiring classification. The LUCAS wetland polygons are derived from multiple multispectral satellites including Sentinel from 2016. They provide the most recent and refined polygon outlines that are

publicly available making them suitable to use as the wetland boundary for the satellite-based wetland vegetation classification. The LUCAS wetland polygons for 2016 were used to clip each band to the extent of the polygons, the extent of the LUCAS polygons is shown in Figure 14.

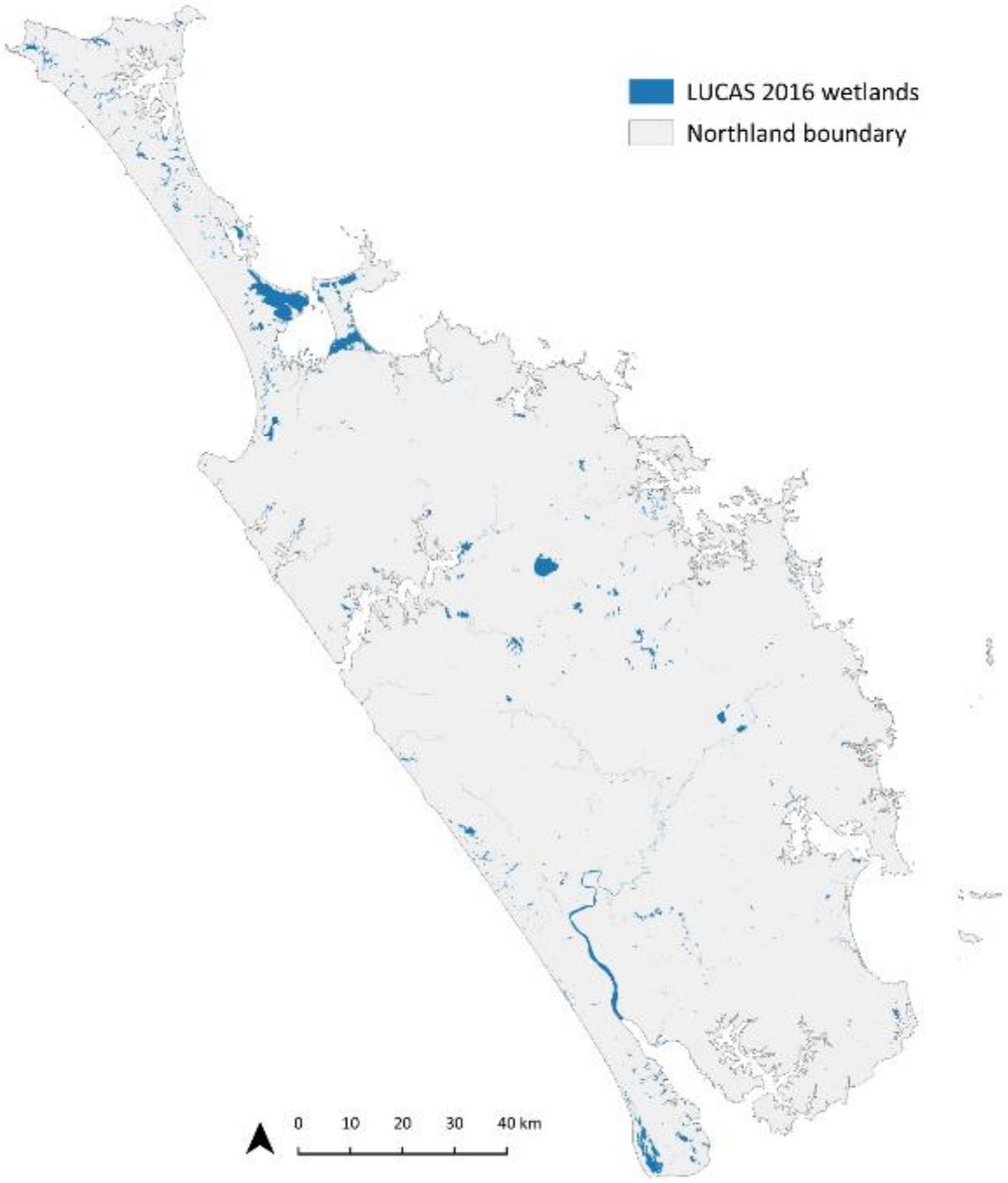

Figure 14: Blue polygons show the extent of the LUCAS polygons used in the segmentation analysis.

The gridded surfaces of the wetland were loaded into SAGA 4.0.0 and the Object Based Image Segmentation (OBIS) tool was used to delineate boundaries of different vegetation types within the wetland polygons. The OBIS tool establishes polygon boundaries by classifying pixels into polygons based on the similarities of spectral signatures. All bands from the visible spectrum and band 8 from the NIR were included in the OBIS applied to Northland. An example of the segmentation is shown below in Figure 15.

Figure 15: A. Wetland area near Kaimaumau, Northland. B. an example of a 20-cluster segmentation based on bands 4, 3, 2 and 8. Different classes correspond to different vegetation patterns suggesting hydrological or successional controls over vegetative cover.

A 20-cluster segmentation was used as a preliminary starting point for segmentation. For Phase 3 it is recommended that segmentation is performed using 40 clusters to better differentiate boundaries within the wetland polygon. Each cluster is associated with a different spectral fingerprint. The 40 clusters will create a higher segmentation rate across all areas. These areas can later be merged if they are determined to be the same. This level of detail cannot be achieved if the image had been under segmented by using a smaller number of clusters.

The wetland boundaries classified by OBIS groups vegetation with similar spectral signatures together, these are consistent with changes in vegetation within the LUCAS wetland boundaries. Figures 16 to 18 show the finer details of wetland composition as a result of the OBIS.

Figure 16: Wetlands west of Kaitaia. A is the OBIS analysis grouping areas that have a similar spectral signature. B shows the outline of the currently mapped wetland extent for comparison.

Figure 17: Wetlands of Pouto, A is the OBIS analysis grouping areas that have a similar spectral signature, this is consistent with changes in vegetation. B shows the outline of the currently mapped wetland extent for comparison.

Figure 18: Wetlands north of Ohia, A is the OBIS analysis grouping areas that have a similar spectral signature, this is consistent with changes in vegetation. B shows the outline of the currently mapped wetland extent for comparison.

Wetland classification by OBIS appears to identify finer grained gradients in vegetation type than provided by existing classifications. However, interpretation of the drivers of variation necessitate the ability to discriminate between hydrological, topographic and land disturbances vectors. The latter will be aided by NRC staff, especially those with knowledge of wetland settings across Northland in Stage 3.

Current limitations of this work relate to the association between vegetative classes and cluster membership. The latter will be addressed under Phase 3 of the work programme.

4 Validation

The resultant relative attenuation layer was qualitatively evaluated against existing classifications of wetlands and hydric soils. Specifically, strong correlations were observed between the attenuation % in both layers and:

1) Northland Regional Councils Top150 wetland polygons (Figure 19)
2) LUCAS land cover wetland polygons (Figure 20)
3) Organic soil orders depicted by Landcare Research's Fundamental Soil Layer (FSL; Figure 21)
4) QMAP geological depiction of peat deposits (Figure 22)
5) Topo 1:50,000 lakes and swamps layer (Figure 23)

Table 3 provides a summary of attenuation % values for each of these pre-existing classifications by polygon size. Future work will include correlation analysis on log transformed and z-scored data between the attenuation % layer and each pre-existing classification.

Table 6: Summary of attenuation % values for each of these pre-existing classifications for polygons less than and larger than 1 ha.

	Mean Att. %	Minimum Att. %	Max Att. %	Std dev. Att. %
Northland Top150 > 1 ha	75.3	44.1	95.7	5.5
Northland Top150 < 1 ha	68.8	39.8	100	2.4
LUCAS Wetlands < 1ha	69.5	0.1	100	5.7
LUCAS Wetlands > 1ha	60.0	0	100	5.5
FSL Organic soil > 1 ha	29.5	0	100	8.0
QMAP peat > 1ha	71.6	40.8	97.9	5.2
Topo1:50,000 lake < 1ha	73.2	0	99.9	4.9
Topo1:50,000 lake > 1ha	60.8	0	100	5.6
Topo1:50,000 swamp < 1ha	70.0	20.0	100	5.5
Topo1:50,000 swamp > 1ha	65.4	18.5	100	4.4

4.1 Qualitative Evaluation

Extended examples of the spatial relationships between the attenuation % layer and Northland's wetlands, organic soils and lakes were demonstrated to NRC staff and feedback sought around areas of interest.

It was noted that attenuation % mapping: (i) provided a finer grained depiction of hydrological gradients than existing classifications; (ii) was detecting areas of former wetland or areas of wet ground that had not been included in previous classifications (such as Fundamental Soil Layer (FSL), Q-Map, LUCAS and Topo150) and; (iii) was able to resolve fine scale variation occurring within wetland (Figure 20) and FSL polygons (Figure 21).

Northland Regional Councils Top150 wetland polygons

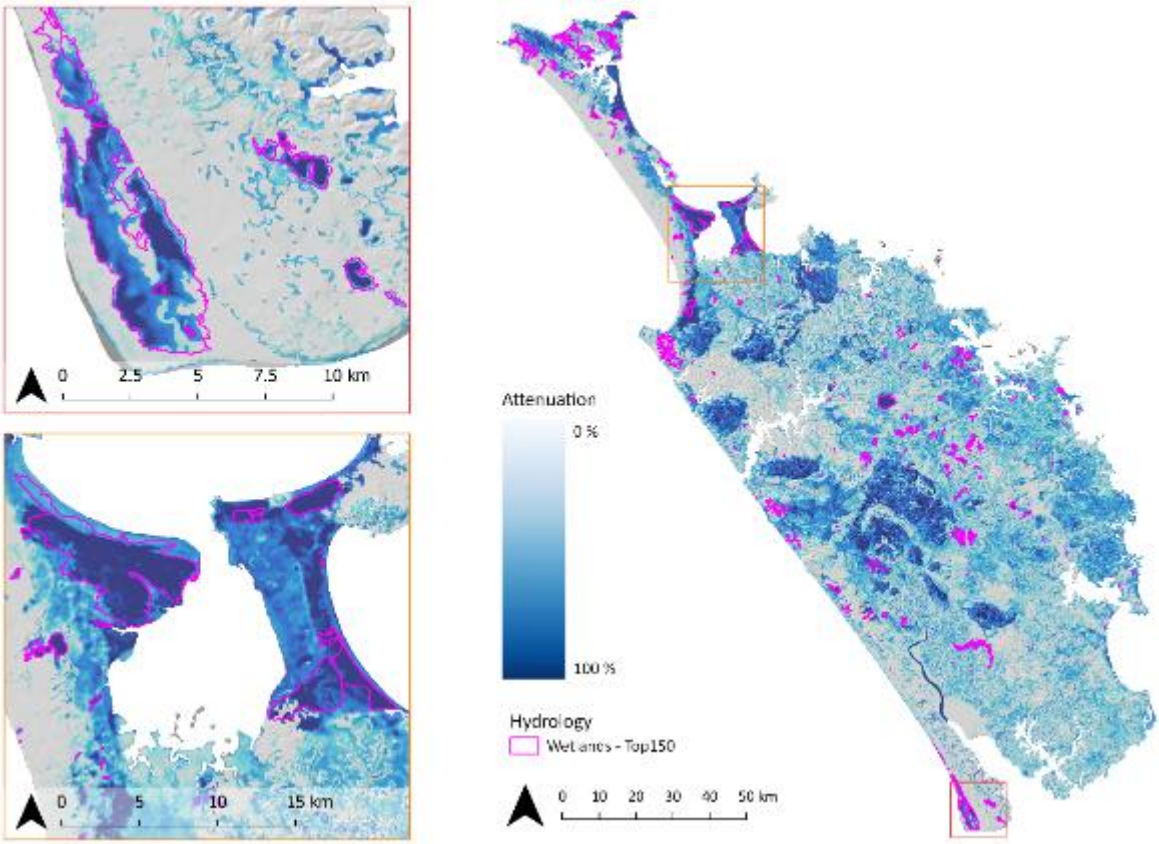

Figure 19: Spatial relationships between attenuation (%) and Northland Regional Councils Top150 wetland polygons.

LUCAS land cover wetland polygons

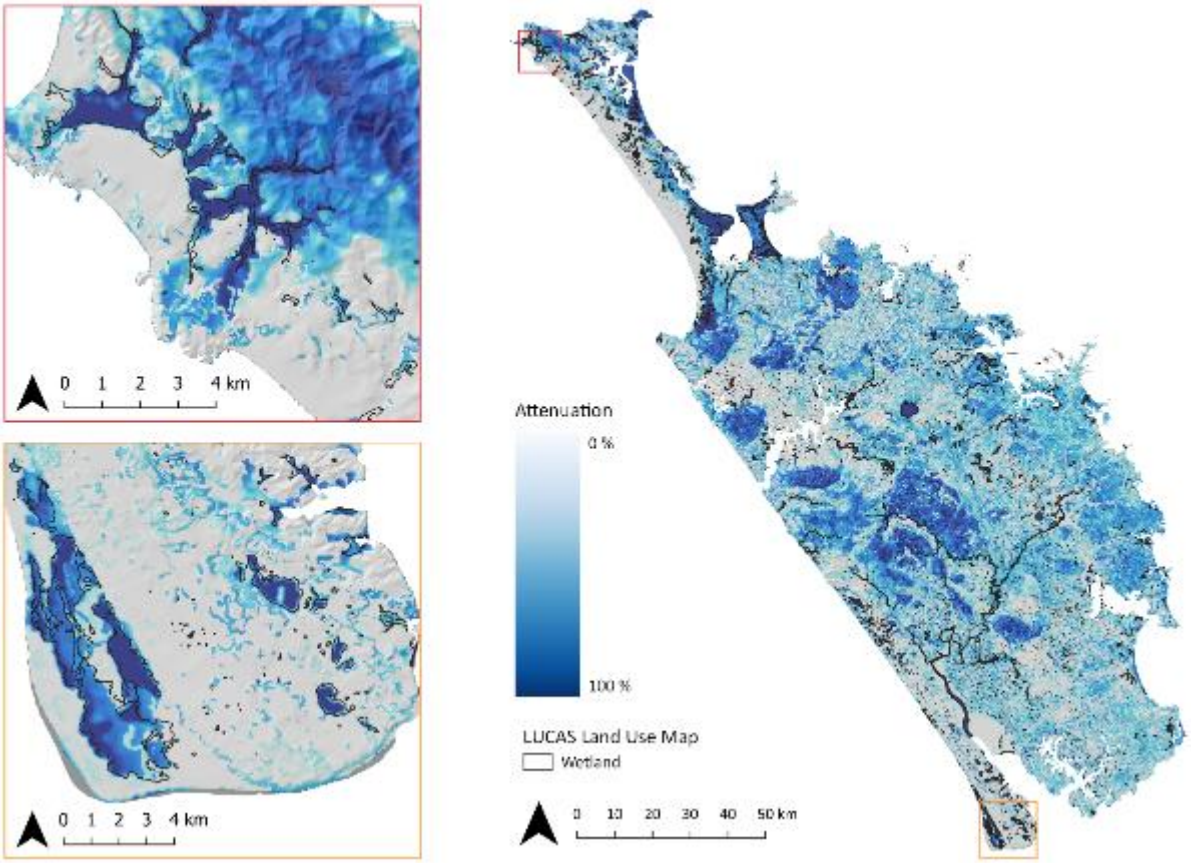

Figure 20: Spatial relationships between attenuation (%) and wetland polygons within the LUCAS NZ Land Use Map 2016 v006.

Fundamental Soil Layer Organic Soil polygons

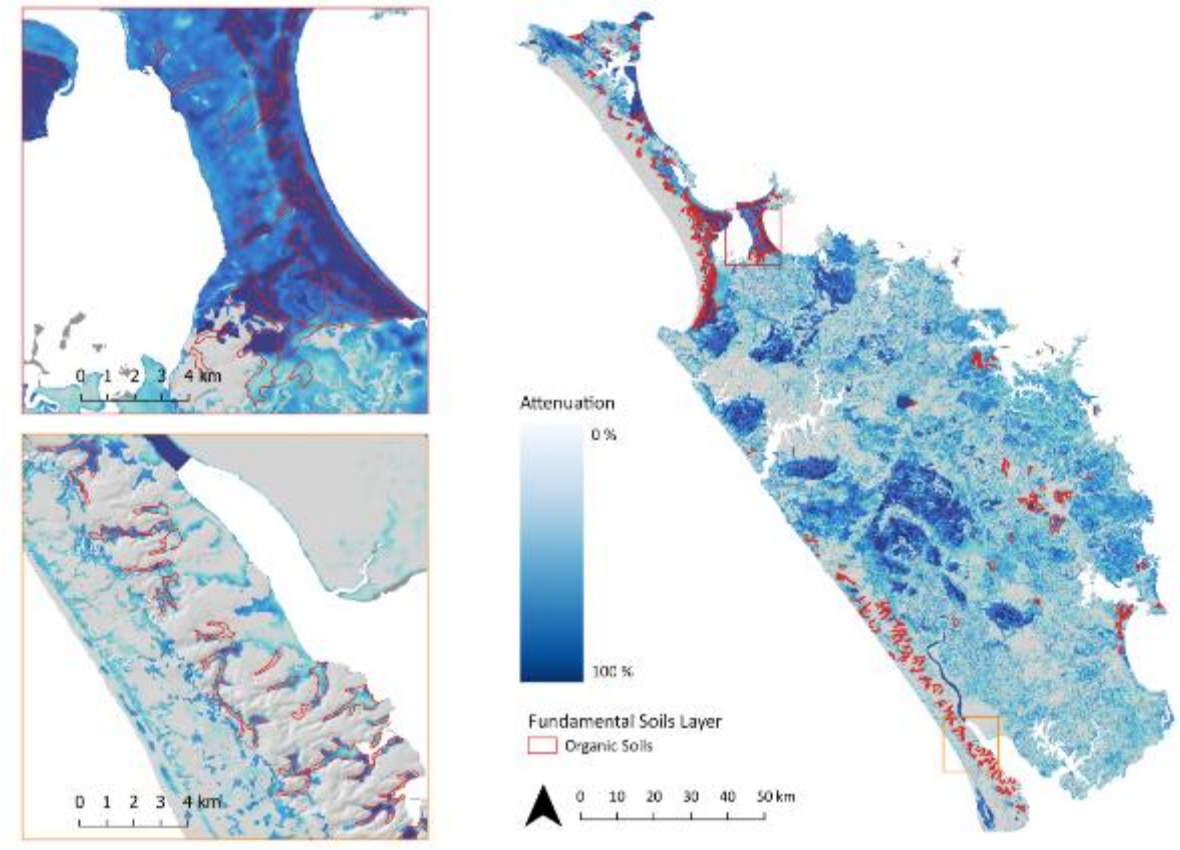

Figure 21: Example of spatial relationship between Organic soil order polygons of the Fundamental Soil Layer and relative attenuation (%).

Q-Map geological depiction of peat deposits

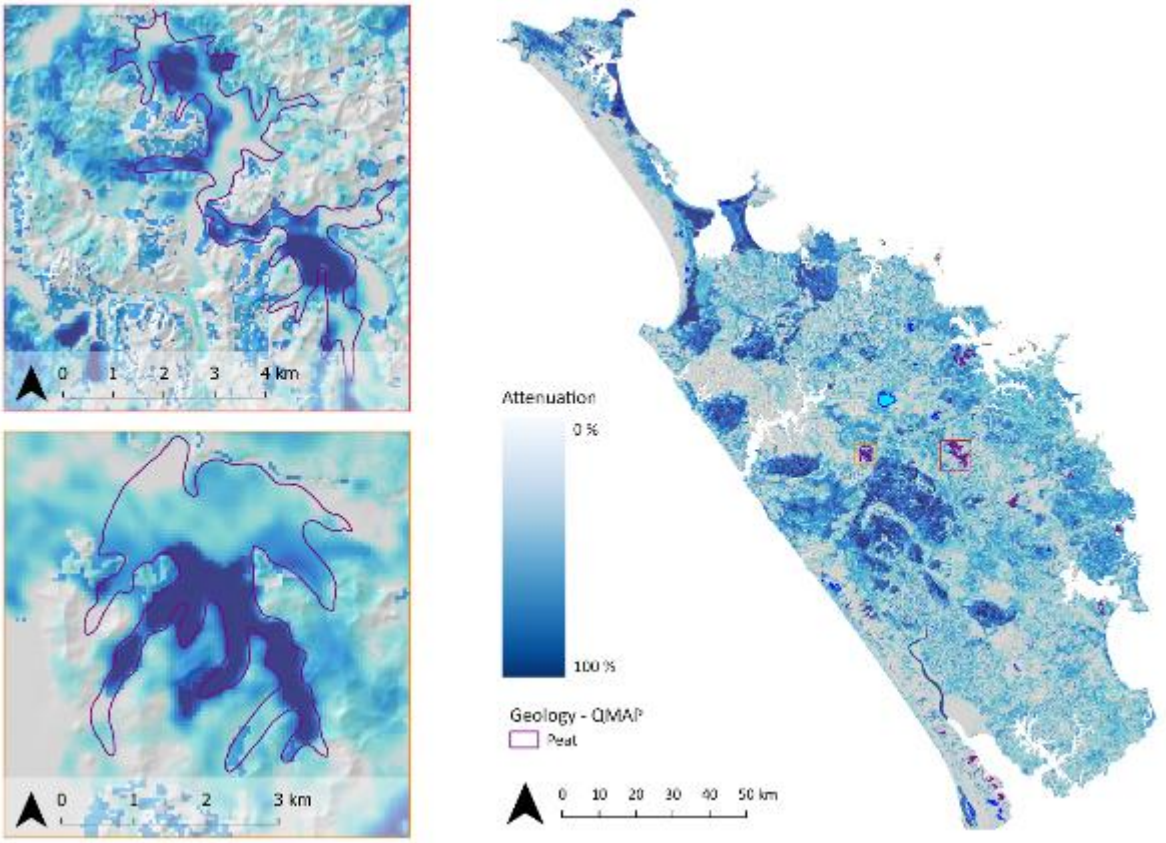

Figure 22: Example of spatial relationship between main 'rock type' as Peat from Q-Map and the relative attenuation (%). Although peat is more correctly defined as a biological sediment it is listed under the 'main rock' designation within Q-Map.

Topo 1:50,000 lakes and swamps layer

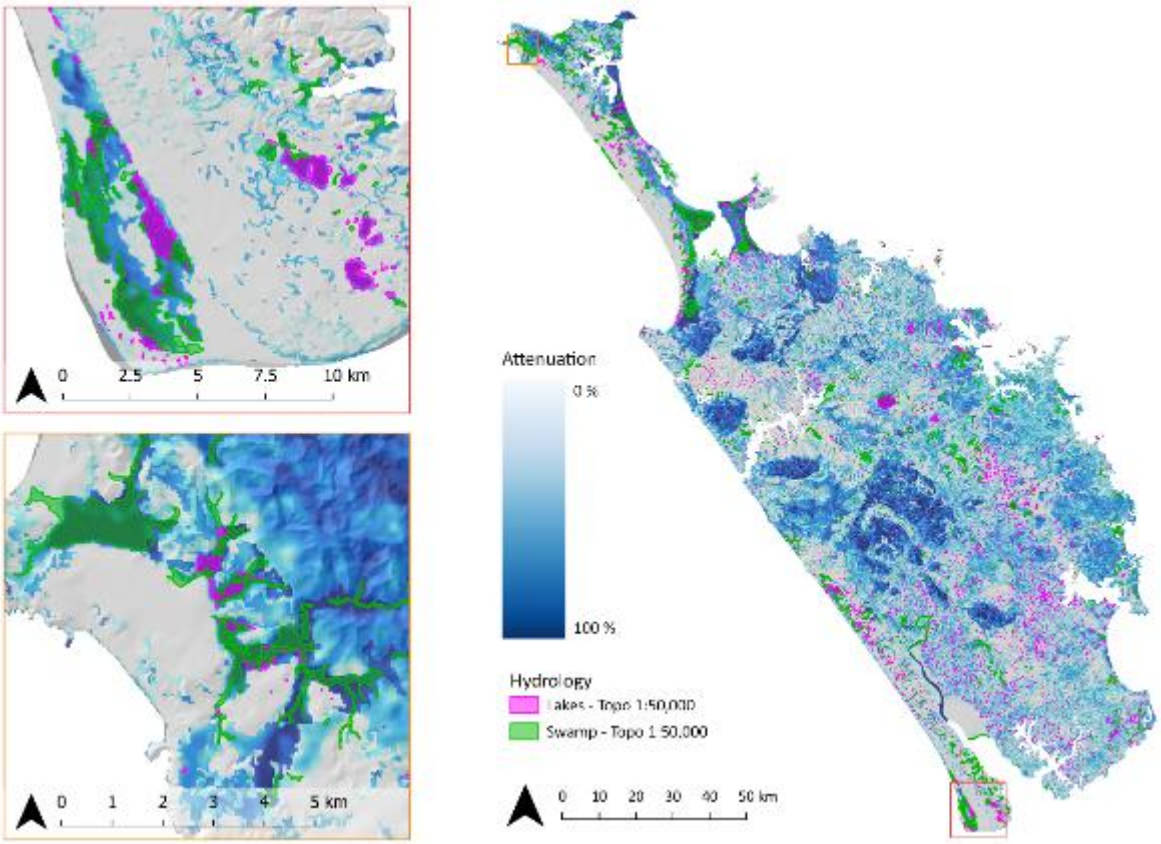

Figure 23: Example of spatial relationship between Topo1:50,000 lakes (pink) and swamps (green) layers and the relative attenuation (%).

4.2 Workshop example - Otakairangi Wetland

Areas of the current Otakairangi Wetland and the former adjacent wetland on private land are identified in Figure 24. This figure also outlines the transect of the Terrain Profile tool which shows the attenuation % across both wetlands.

The points of interest include:

- An open ditch drain through the centre of the Otakairangi Wetland (as identified by the yellow square). This area shows how the attenuation drops from close to 100% to approximately 90% at the drain.

- The land between the Otakairangi Wetland and former wetland (yellow triangle). The attenuation drops to approximately 60%.

- The attenuation % at the drained former wetland is around 80% before the transect moves into the nearby hill country (yellow circle) where the attenuation % falls below 50%.

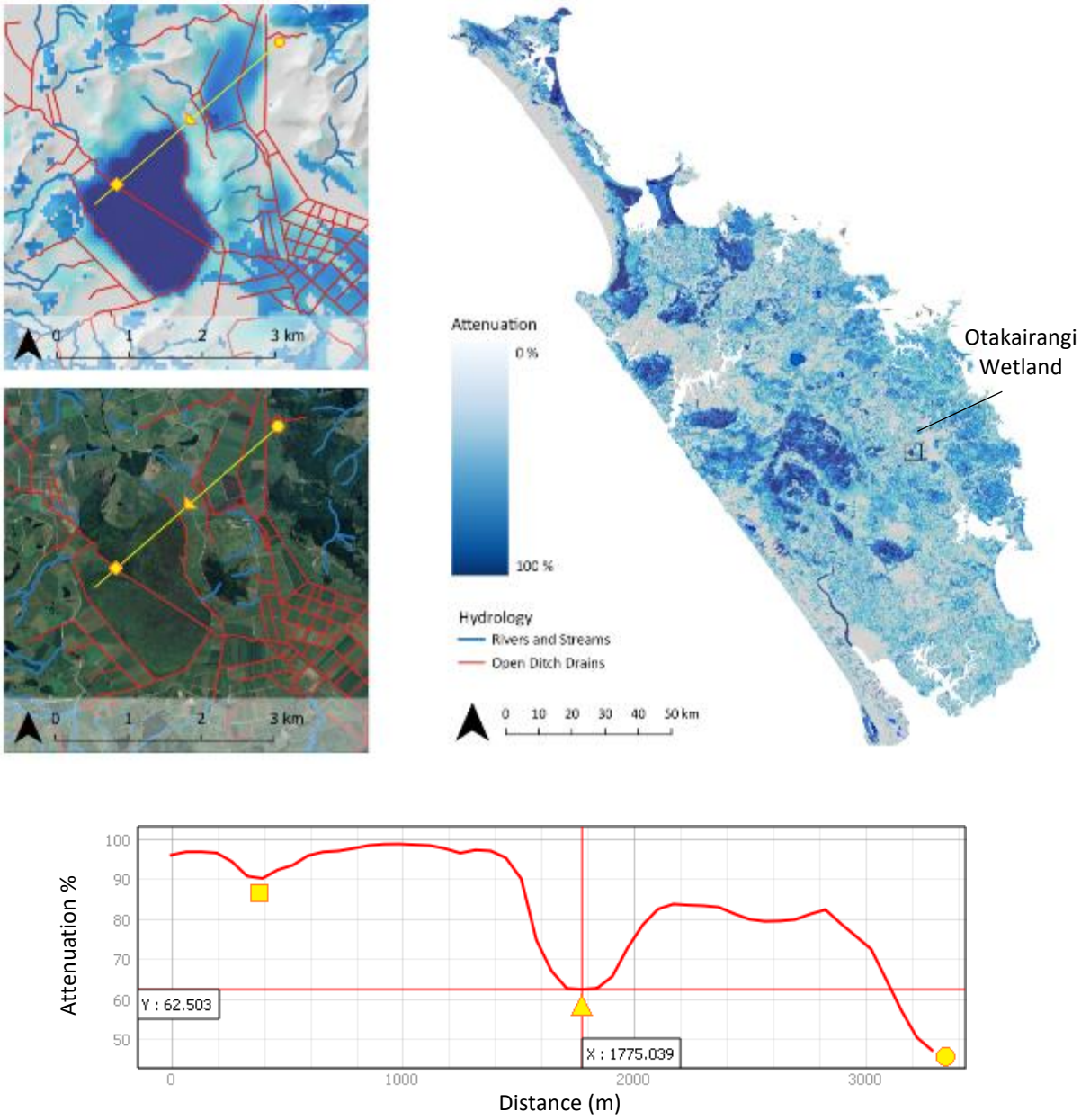

Figure 24: Relative attenuation (%) of the Otakairangi Wetland and the adjoining drained former wetland. Transect of the Terrain Profile tool is shown as the yellow line with adjacent shapes showing areas of interest.

4.3 Limitations

Limitations of this work relate to the:

(i) Timing of the radiometric survey. Specifically, it was conducted during what was a drought year so that gradients likely reflect only the perennially wet parts of the landscape. As such areas of ephemeral wetness, typically winter wet, may not have been detected by the survey.

(ii) The need to further refine the geological boundaries for several units to improve the contrast of the Attenuation % layer. Specifically, Neogene sediments of the Awhitu Group show a large degree of variation that relates to the source of windblown sand.

(iii) Despite its strong performance, deviation from the primary geochemical signature of a rock or sediment also occurs in response to weathering. As such, a component of the attenuation represented here is due to weathering of the primary rock and sediment. There are various ways to correct for the influence of weathering in order to further refine the % attenuation layer for Northland.

(iv) Due to the naturally low Total Count of the Tangihua volcanics partial masking of gamma ray emissions by dense forest cover (c. 12 – 22%) may potentially overestimate attenuation due to volumetric water content. However, consultation with NRC staff suggest that these high rates of attenuation across these areas are spatially coincident with Kauri gumlands.

(v) Floodplain deposits derived from areas of low Total Count that overlap high Total Count sediments at lower altitudes could be refined by developing capture zones for drainage basins. Specifically, provision of capture zone specific zonal statistics for floodplain sediments would enable the alluvial deposits of the region to be further subdivided, providing greater contrast in % attenuation across floodplains where the water table is often elevated.

5 Phase 3 Integration

Phase 3 of this works seeks to integrate radiometric with sentinel satellite data classifying vegetative cover. Future work would benefit from the development of capture zones and flow accumulation vectors from regional Li-DAR to better support finer scale gradients governing the spatial variation in % attenuation identified by this work. Li-DAR could also be used to better define capture zones governing sediment source and geochemical provenance which would enhance the current % attenuation layer and provide additional constraint over sediment source and sink as well as the degree of weathering of the regolith.

References

Beamish, D. (2013a). Gamma ray attenuation in the soils of Northern Ireland, with special reference to peat. Journal of Environmental Radioactivity, 115, 13–27. https://doi.org/10.1016/j.jenvrad.2012.05.031

Beamish, D. (2013b). Peat mapping associations of airborne radiometric survey data. Remote Sensing, 6(1), 521–539. https://doi.org/10.3390/rs6010521

Beamish, D. (2014). Peat Mapping Associations of Airborne Radiometric Survey Data, 521–539. https://doi.org/10.3390/rs6010521

Beamish, D. (2015). Relationships between gamma-ray attenuation and soils in SW England. Geoderma, 259–260, 174–186. https://doi.org/10.1016/j.geoderma.2015.05.018

Beamish, D. (2016). 19. Soils and their radiometric characteristics, (2011). https://doi.org/10.3318/978-1-908996-88-6.ch19

Cook, S.E., Corner, R.J., Groves, P.R. and Grealish, G.J. (1996). Use of airborne gamma-radiometric data for soil mapping. Australian Journal of Soil Research 34, 183–194.

Civco, D., Hurd, J., Prisloe, S., & Gilmore, M. (2006). Characterization of coastal wetland systems using multiple remote sensing data types and analytical techniques. Paper presented at the 3442-3446. doi:10.1109/IGARSS.2006.883.

Edbrooke, S.W. (compiler) (2001). Geology of the Auckland area: scale 1:250,000. Lower Hutt: Institute of Geological & Nuclear Sciences Limited. Institute of Geological & Nuclear Sciences 1:250,000 geological map 3. 74 p. + 1 folded map

Edbrooke, S.W. and Brook, F.J. (compilers) (2009). Geology of the Whangarei area: scale 1:250 000. Lower Hutt: GNS Science. Institute of Geological & Nuclear Sciences 1:250,000 geological map 2. 68 p. + 1 folded map

Grasty, R.L., Minty, B.R.S. (1995). A guide to the technical specifications for airborne gamma-ray surveys. AGSO Australian Geological Survey Organisation, Record 1996/60.

Gatis N., Luscombe D.J., Carless D., Parry L.E., Fyfe R.M., Harrod T.R., Brazier R.E., Anderson K. (2019). Mapping upland peat depth using airborne radiometric and lidar survey data. Geoderma, 335, 78–87. https://doi.org/10.1016/j.geoderma.2018.07.041

IAEA (2003). Guidelines for radioelement mapping using gamma ray spectrometry. International Atomic Energy Agency, Vienna, Technical Report Series, No. 136.

Isaac, M.J. (compiler) (1996). Geology of the Kaitaia area: scale 1:250,000. Lower Hutt: Institute of Geological & Nuclear Sciences. Institute of Geological & Nuclear Sciences 1:250,000 geological map 1. 44 p. + 1 folded map

Kaplan, G., & Avdan, U. (2017). MAPPING AND MONITORING WETLANDS USING SENTINEL-2 SATELLITE IMAGERY. ISPRS Annals of Photogrammetry, Remote Sensing & Spatial Information Sciences, 4.

Løvborg, L. (1984). The Calibration of Portable and Airborne Gamma-ray Spectrometers - Theory, Problems and Facilities. Risø Report M-2456. p. 207.

Pickup, G., and Marks, A. (2000). Identifying large-scale erosion and deposition processes from air-borne gamma radiometrics and digital elevation models. Weathered Landscape. Earth Surface Processes and Landforms, 25, 535–557.

Rawlins, B.G., Lark, R.M., Webster, R. (2007). Understanding airborne radiometric survey signals across part of eastern England. Earth Surf. Process. Landf. 32, 1503–1515. https://doi.org/10.1002/esp.1468.

Rawlins, B.G., Marchant, B.P., Smyth, D., Scheib, C., Lark, R.M., Jordan, C. (2009). Airborne radiometric survey data and a DTM as covariates for regional scale mapping of soil organic carbon across Northern Ireland. Eur. J. Soil Sci. 60, 44–54. https://doi.org/10.1111/j.1365-2389.2008.01092.x.

Scherler, D., Leprince, S., and Strecker, M. R. (2008). Glacier-surface velocities in alpine terrain from optical satellite imagery—Accuracy improvement and quality assessment. Remote Sensing of Environment, 112(10), 3806-3819. doi:10.1016/j.rse.2008.05.018.

Stagpoole, V.M., Edbrooke, S.W., Christie, A.B., Davy, B.W., Caratori Tontini, F., Soengkono, S., Cox, S.C., Isaac, M.J. (2012). Northland airborne magnetic and radiometric survey: a geological interpretation. Lower Hutt, N.Z.: GNS Science. GNS Science report 2011/54 113 p.

Taylor, M.J., Smettem, K., Pracillio, G., Verboom, W. (2002). Relationships between soil properties and high-resolution radiometrics, central eastern Wheatbelt, Western Australia. Exploration Geophysics 33, 95-102.

Wilford, J. (2012). A weathering intensity index for the Australian continent using airborne gamma-ray spectrometry and digital terrain analysis. Geoderma, 183–184, 124–142. https://doi.org/10.1016/j.geoderma.2010.12.022